Conformational Behavior of Poly(L-lactide) Studied by Infrared Spectroscopy

E. Meaurio, E. Zuza, N. López-Rodríguez, and J. R. Sarasua*

The School of Engineering, The University of Basque Country (EHU-UPV), Alameda de Urquijo s/n. 48013 Bilbao, Spain

Received: September 14, 2005; In Final Form: January 23, 2006

This paper reports the analysis of the C═O stretching region of poly(L-lactide). This spectral band splits into up to four components, a phenomenon that a priori can be explained in terms of carbonyl−carbonyl coupling or specific interactions (such as C−H···O hydrogen bonding or dipole−dipole). Hydrogen bonding can be discarded from the analysis of the C−H stretching spectral region. In addition, low molecular weight dicarbonyl compounds of chemical structure similar to that of PLLA, such as diacyl peroxides, show a remarkable splitting of the carbonyl band attributed to intramolecular carbonyl−carbonyl coupling. Several mechanisms can be responsible for this behavior, such as mechanical coupling, electronic effects, or through-space intramolecular TDC (transition dipole coupling) interactions. Intermolecular dipole−dipole interactions (possible in the form of interchain TDC interactions) are proven to be of minor relevance taking into account the spatial structure of the PLLA conformers. The Simply Coupled Oscilator (SCO) model, which only accounts for mechanical coupling, has been found to predict adequately the relative intensity of the symmetric and asymmetric bands of dicarbonyl compounds. The dispersion curves predicted for PLLA by the SCO model also match those given by more general treatments, such as Miyazawa's first-order perturbation theory. Hence, the SCO model is adopted here as an adequate yet simple tool for the interpretation of band splitting caused by intramolecular coupling of polylactide. The four components observed in the C═O stretching band of semicrystalline PLLA are attributed to the four possible conformers: gt, gg, tt, and tg. The narrow bands observed for the interlamellar material are attributed to highly ordered chains, indicating the absence of a truly amorphous phase in the crystalline polymer. The interphase seems to extend over the whole interlamellar region, showing the features of a semiordered metastable phase. In amorphous PLLA, bands corresponding to gt, gg, and tt conformers also can be resolved by second derivative techniques, and curve-fitting results provide information about the conformational population at different temperatures.

Introduction

Polylactides are biodegradable polymers that attract much attention because of their environmental benefits.[1] Poly(L-lactide), PLLA, is obtained from renewable resources and its industrial scale production has begun recently.[2] This material is also well-known in the medical industry as a biocompatible polymer for applications such as drug delivery systems,[3] implant materials for bone fixation,[4] and surgical suture.[5] But the main reason behind its debut in large-scale production is found in its tremendous potential in traditional applications where thermoplastics are employed, such as the production of disposable products for the packaging and film industries.[6] Finally, PLLA is also melt-spinnable and has very good fiber- and film-forming properties. Recently, applications involving high-strength fibers and films were reported.[7]

Many aspects of PLLA, such as its crystallization behavior, present exciting areas for research. It was pointed out that two crystalline structures, α and β, existed in solution-spun PLLA.[7] At low drawing temperatures or low draw ratios, the pseudoorthorhombic α structure is obtained containing 10_3 helices. At higher drawing temperatures and/or higher draw ratios, an orthorhombic β structure is obtained containing 3_1 helices. There appears to be no definitive determination of the crystalline structure for a bulk sample.

If the crystalline structure remains poorly defined, studies regarding the amorphous phase are even scarcer. Tonelli et al. developed a rotational isomeric state (RIS) model of PLLA from which conformational energy maps were developed and the distribution of conformer population was calculated.[8] In a recent work the distribution of conformers predicted by Tonelli has been reexamined by comparison of simulated and experimental Raman spectra, but this study allowed only a qualitative comparison.[9] In this paper, conformational changes observed in both crystalline and amorphous PLLA samples are examined by FTIR spectroscopy, a technique a priori sensitive to specific interactions, morphology, and conformation.

The carbonyl stretching region of polylactides has been reported to show conformational sensitivity.[10] In addition, it also can be affected by specific interactions[11] and morphology. Taking into account the chemical structure of PLLA the only possible specific interactions are C−H···O hydrogen bonding and dipole−dipole interactions. Recently, it has been proved that hydrogen bonding is not observed in PLLA, although these interactions were confirmed in the stereocomplex obtained from the stoichiometric blend of both polylactide stereoisomers.[12,13] Regarding the possibility of dipole−dipole interactions, in a recent paper the spectral features observed in the C═O stretching region have been attributed to correlation field splitting arising from interchain dipole−dipole interaction between C═O groups.[14] However, this interpretation is not consistent with the fact that correlation field splitting is only observed at room temperature

* Address correspondence to this author. E-mail: jr.sarasua@ehu.es.

10.1021/jp055203u CCC: $33.50
Published on Web 03/01/2006

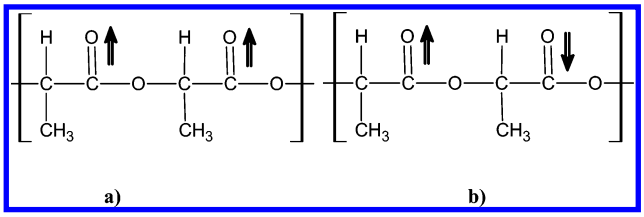

Figure 1. (a) Symmetric and (b) asymmetric carbonyl stretching modes for a hypothetical isolated lactide dyad.

in the ($-CH_2-$) bending vibrations and in the ($-CH_2-$) rocking modes, but is not observed in C═O groups.[15] Dipole−dipole interactions can nevertheless contribute to the shape of the C═O stretching band through transition dipole coupling (TDC) interactions, as proposed by Krimm et al. to explain the splitting observed in the amide stretching band of polypeptides.[16−19]

IR spectroscopy is also sensitive to morphology. From a theoretical point of view, crystallization alone does not affect the location of any spectral band, but the intensity of IR bands can vary due to changes in density and refractive index.[20] Hence, for a nonautoassociating crystallizable polymer, crystallization results in narrow bands (due to molecular order within the crystalline domains) located at the same wavenumber as the original band, and with slightly higher absorptivities. However, in many systems crystallization is accompanied by the development of specific interactions or by conformational changes. Thus, spectral changes observed during crystallization will actually reflect the interaction and/or conformational changes occurring during the crystallization process. The effect of specific interactions in the spectral bands sensitive to morphology becomes evident for strongly autoassociated systems. For example, in polyamides and polyurethanes the crystalline band shifts to lower wavenumbers and its absorptivity increases noticeably.[21] Both the red shift and the absorptivity increase are a consequence of the strength of the specific interactions developed during crystallization.[22,23] Note also that specific interactions can also occur in systems for which they were traditionally discarded. For example, the occurrence of C−H···O hydrogen bonding has not been accepted until recent years, but Taylor and Kennard[24] gave evidence from crystallographic data of the existence of C−H···O contacts in many systems for which autoassociation was not traditionally accepted. In addition to hydrogen bonding, TDC interactions also have been claimed to explain morphology dependent frequency shifts observed in poly(oxymethylene) (POM), poly(ethylene oxide) (POE), and poly(tetrafluoroethylene) (PTFE).[25,26]

In the particular case of PLLA, experimental findings in low molecular weight compounds of similar structure are of special interest. If two C═O are connected by one C−C bond, mechanical coupling occurs and splitting of the C═O stretching band in a symmetric and an asymmetric band is observed.[27] When two or more C−C bonds connect the carbonyl groups, splitting is not observed. However, when the C═O groups are connected by atoms carrying unshared electron pairs (N, O), as shown in succinimides, anhydrides, and peroxides of organic acids, considerable splitting with enhanced intensity of the ν_{as} peak in the infrared spectra appears.[28] The chemical structure of PLLA is very similar to that of diacyl peroxides, but an oxygen atom is replaced by a carbon atom (Figure 1). There is only a C−C bond between neighboring C═O groups, connected to an oxygen atom, that according to experimental results is a good transmitter of vibrational coupling.[28−32] Hence, conformational sensitivity due to intramolecular coupling of C═O groups can be expected in PLLA, according to its structural similarity with diacyl peroxides. In addition, the possible influence of intermolecular transition dipole coupling (TDC) interactions also should be considered for a proper interpretation of the experimental spectra.

Regarding the mechanism for the intramolecular interaction, Popov et al.[28] found by normal mode calculations that mechanical coupling can account only for a limited portion of the observed splitting in the aforementioned low molecular weight compounds. They attributed the enhanced splitting to electronic effects between the electron donor atoms (O or N atom between C═O groups) and the electron acceptor C═O groups. Whatever the case, spectral findings in those compounds prove that the origin of the enhanced spectral splitting is intramolecular coupling.

In contrast to dicarbonyl compounds, coupling in a polymeric chain may be extended through the whole molecule, complicating the interpretation of the observed spectra. To account for the electronic effects proposed by Popov et al.,[28] ab initio calculations should be necessary, but these are beyond the scope of our work. Hence, we will assume a simpler model, the simply coupled oscillator (SCO) model, to simulate the vibrational behavior of the polymeric chain. If coupling is mainly due to intramolecular (through bonds) mechanisms, this model should lead to at least appropriate qualitative predictions.

Experimental Section

A. Starting Materials. Optically pure poly(L-lactide) containing less than 0.01% residual solvent and less than 0.1% residual monomer was supplied by PURAC BIOCHEM (Netherlands). Its specific rotation in chloroform at 20 °C was −157.3°. The molecular weight of poly(L-lactide) was measured viscometrically in a Ubbelohde type viscometer in chloroform at 30 °C, using the relation:[33]

$$[\eta] = (5.45 \times 10^{-4}) M_v^{0.73}\,(\mathrm{dL/g}) \qquad (1)$$

A value of $M_v = 3.2 \times 10^5$ g/mol was obtained.

B. Infrared Spectroscopy. Infrared spectra of blends were recorded on a Nicolet AVATAR 370 Fourier transform infrared spectrophotometer (FTIR). Samples were prepared by casting 0.5 wt % chloroform solutions on KBr pellets, followed by vacuum drying at 50 °C for 48 h. For the melt crystallization studies, the sample was placed in a temperature cell accessory controlled with a Omega Temperature Controller within an accuracy of ±1 °C. The sample was heated at 10 deg/min to 200 °C, held for 2 min to melt the polymer and completely erase the thermal history, and cooled at 5 deg/min to 150 °C for the isothermal crystallization. IR spectra were collected after 1 min intervals during the annealing process, by co-adding 8 scans at a 2 cm^{-1} resolution. Second derivatives of the spectra recorded were smoothed with a quartic 9 point Savitzky−Golay smoothing filter.[34,35] Care was taken on the degree of distortion introduced by the smoothing algorithm, which was checked according to the procedure reported elsewhere.[11]

C. Molecular Modeling. Bond lengths and angles of the RIS model have been transferred from literature and are based on results obtained in structural analysis of esters and the accepted standard values of these parameters in organic molecules.[8,36] The 3D structure has been built with the free software package Arguslab 4.0.1.[37]

Results and Discussion

A. Application of the Simply Coupled Oscillator (SCO) Model to PLLA. According to the results of Popov et al.[28] (see the Introduction), coupling between C═O groups along the

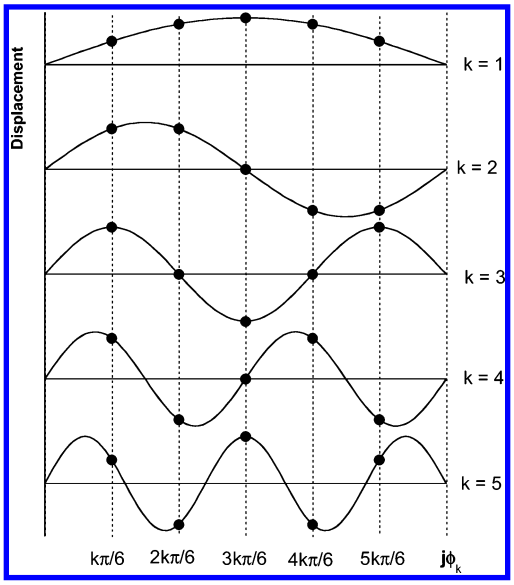

Figure 2. Displacements predicted by the Simply Coupled Oscillator model for a set of $N = 5$ coupled oscillators, where k represents the normal mode and ϕ_k the phase angle.

PLLA chain is expected, resulting in the loss of localization of vibrational modes. In previous works, the simply coupled oscillator (SCO) model has been successfully applied to study the vibrational modes of chains of mechanically coupled oscillators. Already studied systems include coupled CH_2 bending modes in *n*-alkanes[38−41] and nylons,[42,43] and CF_2 stretching modes in perfluoroalkanes.[44,45] Application of this model to the stretching of C═O groups in PLLA means representing the local carbonyl mode by an oscillator of mass m, coupled by springs of constant k in a linear array of N identical oscillators. The theoretical model is solved assuming fixed ends. For a system of N identical coupled objects, N solutions (normal modes) are found. For the kth normal mode, there is a phase difference ϕ_k between consecutive vibrating groups:

$$\phi_k = \frac{k\pi}{(N+1)} \qquad k = 1, 2, ..., N \tag{2}$$

The displacement x_j of the jth particle vibrating in the kth normal mode is given by:

$$x_j = A_t \sin(j\phi_k) \tag{3}$$

The vibrating chain behaves as a standing wave, in which A_t represents the variation of the oscillating amplitude with time, and the sinus term represents the shape of the standing wave along the chain. Figure 2 represents the relative displacements calculated for a chain of $N = 5$ coupled oscillators. The mode with $k = 1$ is an in-phase mode and the mode with $k = 5$ is an out-of-phase mode.

The model can be applied to simulate the spectra in the carbonyl spectral region. The relative transition moment, R, of a single normal mode is related to the product of the displacement and the dipole moment derivative. In addition, the relative infrared intensity is proportional to the square of the transition moment:

$$I \propto R^2 = \left[(r - r_e)\frac{d\mu}{dr}\right]^2 \tag{4}$$

The total transition moment for a normal mode can be obtained from the sum of individual C═O transition moments. The displacements of individual C═O groups are obtained from the SCO model. The dipole moment derivatives are identical for all C═O groups but oriented individually according to the local structure of the chain. Thus, it is necessary to take into account the conformation of the chain.

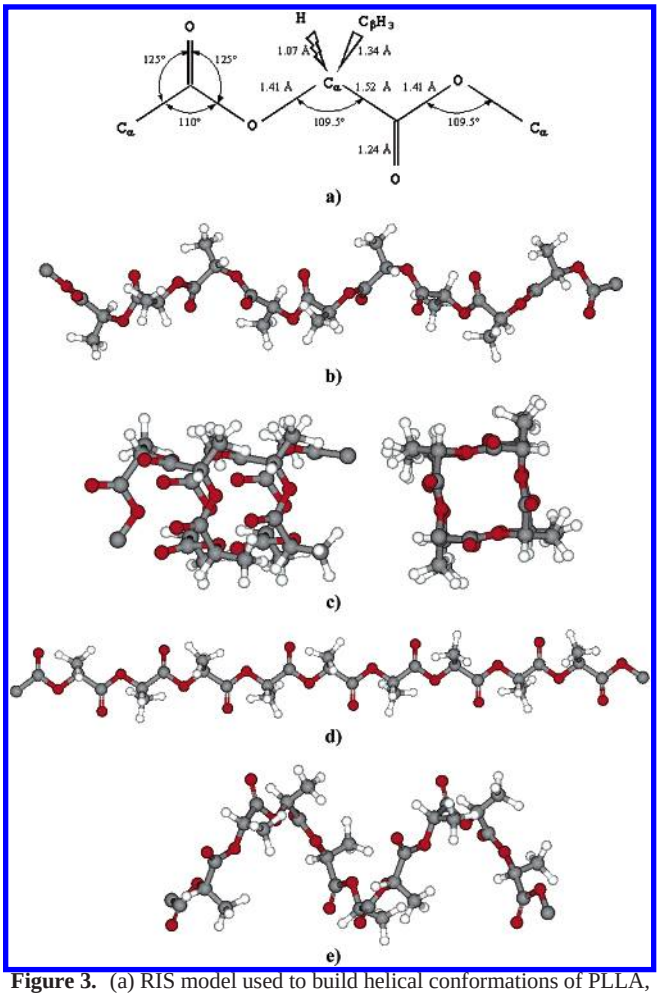

Figure 3. (a) RIS model used to build helical conformations of PLLA, (b) gt helical conformation (103 or 31 helix), (c) gg helical conformation (41 helix), (d) tt helical conformation (21 helix), and (e) tg helical conformation (51 helix).

A rotational isomeric state (RIS) model for poly(L-lactide) and an associated conformational energy map have been developed.[8,36] Three skeletal bonds occur along the molecular chain in poly(L-lactide): C−O (ester), O−C_α, and C_α−C. The C−O (ester) bond is assumed to be always trans due to conjugation with the C═O double bond. The O−C_α bond has two energy minima around −160° and −48°, and the C_α−C bond has two energy minima around 160° and −73°. Since 160° is close to 180°, the 160° angles are termed trans (t). In the same way, −48° and −73° are close to −60° and are termed gauche (g+). The RIS model of PLLA predicts four minimum energy states corresponding to four distinct conformations for the O−C_α and C_α−C bonds: tt (−160°, 160°), tg (−160°, −48°), gt (−73°, 160°), and gg (−73°, −48°). The gt has the lowest energy and corresponds to either a 3_1 or a 10_3 helix. The second lowest energy minimum, gg, takes the shape of a highly compressed 4_1 helix, and its small energy difference of 0.08 kcal/mol is well below the estimated uncertainty of ±0.5 kcal/mol for the theoretical model.[8] According to the calculated contour map, at room temperature a completely random structure would contain 55% gt conformers, 37% gg, and about 4% of either tg and tt. Figure 3 shows the structure of the helical conformers of PLLA, from which the structural parameters

required for spectral calculations will be obtained. Figure 3 also includes the molecular parameters of the RIS model transferred from literature.[8,36]

The SCO model can be applied to these most probable conformations. Let us consider a general helix in the direction of the *Z* axis. For simplicity, we will assume that all C═O groups point to the center of the helix, but this assumption has no effect on the final equation. Let us call θ the angle between the C═O group and the helix axis. The projection of the relative transition moment of a C═O group in the *Z* axis is then $x_j \cos \theta$, and its projection in the *XY* plane is $x_j \sin \theta$. The summation of transition moments in the *XY* plane is a 2D problem. Let us consider a helix in H_a conformation, where *H* represents the number of repetitive units and *a* is the number of turns. To simplify the algebra, the helix is oriented such that the first C═O group is located at an angle of $(2\pi a/H)$ degrees. The next *j*th C═O group will be rotated *j* times an angle $(2\pi a/H)$ in the 2D projection. The relative transition moments in the *X*, *Y*, and *Z* axis directions for the *k*th normal mode are (sign is irrelevant):

$$R_x = \sum_{j=1}^{N} x_j \sin\theta \cos\left(j\frac{2\pi a}{H}\right) \quad (5)$$

$$R_y = \sum_{j=1}^{N} x_j \sin\theta \sin\left(j\frac{2\pi a}{H}\right) \quad (6)$$

$$R_z = \sum_{j=1}^{N} x_j \cos\theta \quad (7)$$

And the relative infrared intensities for the *k*th normal can be obtained from:

$$I_k = (R_x)^2 + (R_y)^2 + (R_z)^2 \quad (8)$$

Thus

$$I_k = \left[\sum_{j=1}^{N} \sin(j\phi_k) \sin\theta \cos\left(j\frac{2\pi a}{H}\right)\right]^2 + \left[\sum_{j=1}^{N} \sin(j\phi_k) \sin\theta \sin\left(j\frac{2\pi a}{H}\right)\right]^2 + \left[\sum_{j=1}^{N} \sin(j\phi_k) \cos\theta\right]^2 \quad (9)$$

Equation 9 is a general expression for any helical chain. If the individual transition moments do not point to the helix axis, the same equation can be deduced if the whole set of transition moments is rotated without changing the direction of the individual vectors until both the transition moments and the *Z* axis are coplanar. This transformation does not change the individual projections in the *Z* axis direction nor in the *XY* plane, and hence leads to the same result. For such helical chains, θ should be defined as the angle between the transition moment and the direction of the helix axis.

In addition to eq 9, absorption wavenumbers are also needed to plot simulated spectra, but there is no simple model allowing their calculation. Fortunately, in coupled systems, the absorption frequency is related to the phase angle ϕ of the normal mode by unique dispersion curves, hence, a plot of intensity versus phase angle can be regarded as an equivalent form of a real spectrum.[38−45] Figure 4 displays simulated spectra for different model chains. First, let us consider the spectra predicted for helixes of different length, with C═O groups normal to the helix axis ($\theta = 90°$). Figure 4a displays the simulated C═O group spectrum for a dyad of gt conformers (equivalent to a 3_1 helix with $N = 2$). The spectrum shows a symmetric band ($\phi = 60°$) and an asymmetric band ($\phi = 120°$), with a relative intensity I_s:Ia_s equal to 1:3. This value is in good agreement with experimental results for dicarbonyl compounds, for which typical intensity ratios range from 1:2 to 1:4,[32] supporting the qualitative value of the model. As the number of coupled oscillators increases (see Figure 4, panels b and c), the individual bands predicted, termed progression bands, concentrate around a phase angle $\phi = 2\pi a/H$ (120° for a 3_1 helix). Extrapolation of the spectrum shown in Figure 4c to a real spectrum obtained at room temperature in an amorphous polymer should lead to a single band, because typical widths for individual components are about 20 cm^{-1}, and the expected coupling interaction involves a shift lower than 0.5 cm^{-1} per phase angle degree. Hence, a model with $N = 11$ coupled oscillators will be used for spectral simulation. It also should be noted that the SCO model is only valid for regular arrangements of coupled oscillators, a situation that for values of *N* exceeding some units is only expected in the crystalline phase. Thus, as a first approximation, the predicted spectra with $N = 11$ will be considered valid for regular arrangements of conformers.

Figure 4d shows the spectrum obtained for a 10_3 helical chain with C═O groups forming an angle $\theta = 60°$ with the helix axis. This spectrum is equivalent to the one predicted for the crystalline phase of PLLA from group theory analysis by Kister et al.,[10] indicating the presence of two bands, one with A symmetry (the transition moment along the helix axis), and one with E symmetry (the transition moment perpendicular to the helix axis), which is doubly degenerate. In addition, Figure 4e shows the spectrum obtained for a PLLA chain in the 10_3 helical conformation obtained from the RIS model, for which a value $\theta = 80.9°$ is measured. As can be seen, the absorption due to the A mode is negligible, and the model predicts only a single band, because C═O groups are nearly perpendicular to the helix chain. Note that group theory analysis predictions are qualitative, but the calculation based on the RIS model has quantitative value.

Panels f−h in Figure 4 show the spectra calculated from eq 9 for the other conformers. Figure 4f is the spectrum of the gg conformer ($N = 11$, $\theta \approx 0°$, $H_a = 4_1$). The transition moment of this helical conformation is parallel to the *Z* axis, and as expected absorption is only predicted for the in-phase mode (higher wavenumbers). Figure 4g is the spectrum for the tt conformer ($N = 11$, $\theta \approx 90°$, $H_a = 2_1$). As expected, the model predicts absorption only for the out-of-phase mode. Finally, Figure 4e is the spectrum for the tg conformer ($N = 11$, $\theta \approx 90°$, $H_a = 5_1$), predicting a band located at $\phi = 72°$. In addition, the SCO model predicts identical absorptivities for all the PLLA conformers.

Although from the point of view of the SCO model spectra in Figure 4 are valid only for regular arrangements of conformers, they also serve as reference for the interpretation of the spectrum of the amorphous phase, as suggested by Snyder et al. in the study of perfluoroalkanes.[45] These compounds adopt a 13_6 helix, in which coupling is observed for the symmetric stretching mode (ν_3) of CF_2 groups. In the crystalline phase at low temperatures, perfluoroalkanes show progression bands with relative intensities adequately predicted by the SCO model.[44] In going from ordered to disordered chains, the bands in the ν_3 region tend to form a pattern similar to the well-defined pattern observed for ordered chains; although the spectrum of the amorphous sample contains broader bands due to new spectral

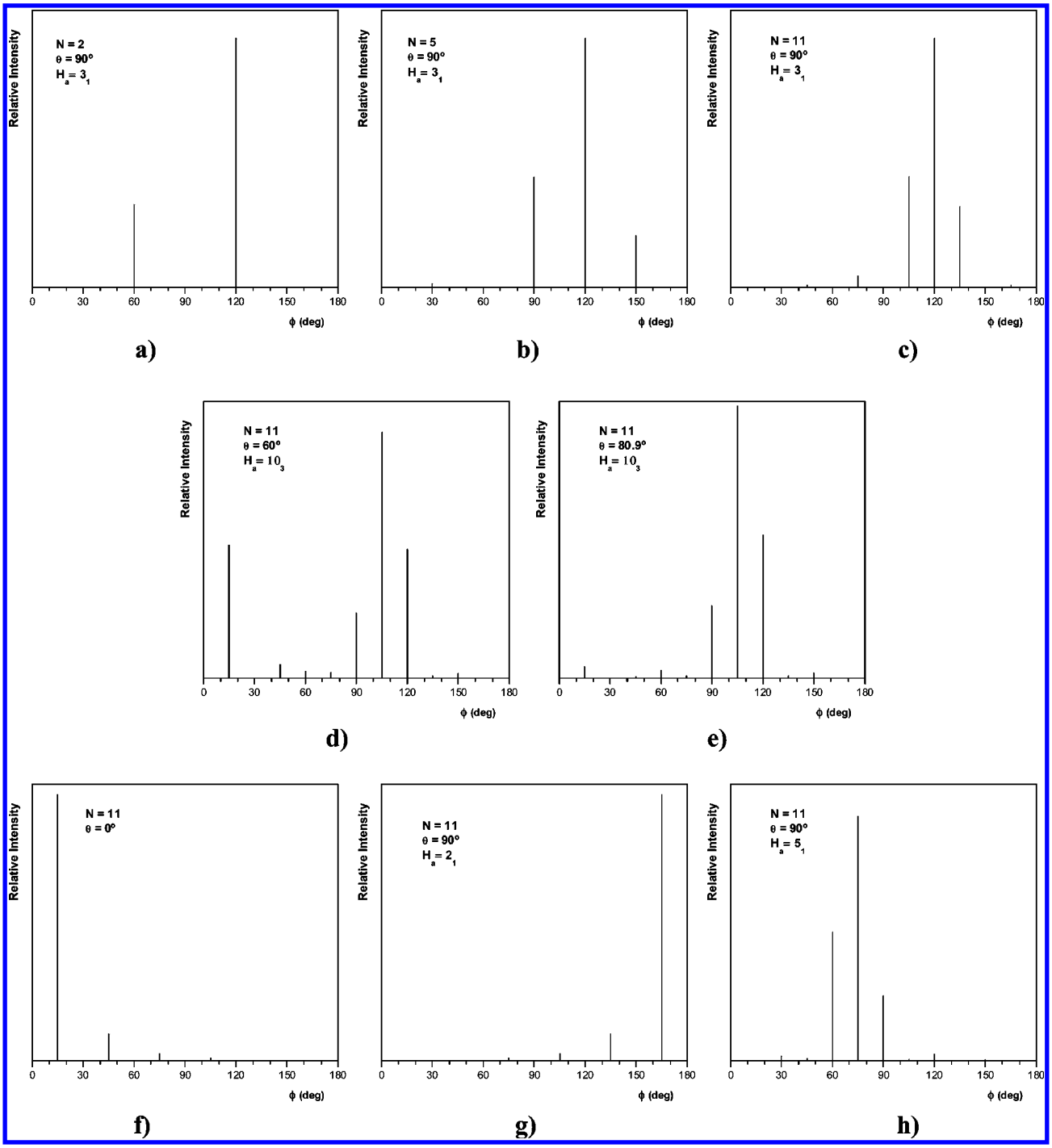

Figure 4. Spectra calculated for PLLA conformes with the SCO model. Spectra a−c have been calculated for 3_1 helical conformations with $\theta = 90°$. As can be observed, spectrum a resembles the experimental result for dicarbonyl compounds. Going from spectra a to c, the calculated spectrum tends to a single band located at a phase angle $\phi = 2\pi a/H$. Spectrum d simulates the spectrum of a hypothetical 10_3 helix with $\theta = 60°$. Spectrum e shows the real situation for PLLA ($\theta = 80.9°$), where the absorption predicted for the A mode is negligible. Spectra f, g, and e are predicted for gg, tt, and tg helical conformations.

contributions forming clusters around the original ν_3 frequencies. In addition, the integrated intensity of the ν_3 bands does not show significant changes during the ordering/disordering process. The trends reported by Snyder et al. in perfluoroalkanes should hold for PLLA, hence the SCO model results in Figure 4 provide the basis to interpret the spectra of either amorphous or crystalline phases in PLLA.

B. C═O Stretching Region of Crystalline PLLA. First, we will discuss the spectral features of PLLA during crystallization, because the spectrum of crystalline PLLA shows sharp well-resolved features. Figure 5 displays the spectrum of PLLA during crystallization. The second derivative spectrum of amorphous PLLA at 150 °C presents two broad bands, at about 1776 and 1755 cm^{-1}. According to Tonellis calculations,[8] the population distribution at this temperature is 8% of tt conformers, 7% tg, 35% gg, and 50% gt. As a first approximation, it seems rationale to assign the observed spectral bands mainly to the two dominant conformers (gg and gt), and because gg conformers absorb at higher wavenumbers (Figure 4), the band at 1776 cm^{-1} is assigned to gg conformers and the band at 1755 cm^{-1} to gt conformers. Important spectral changes are observed in the carbonyl region as crystallization proceeds. The second

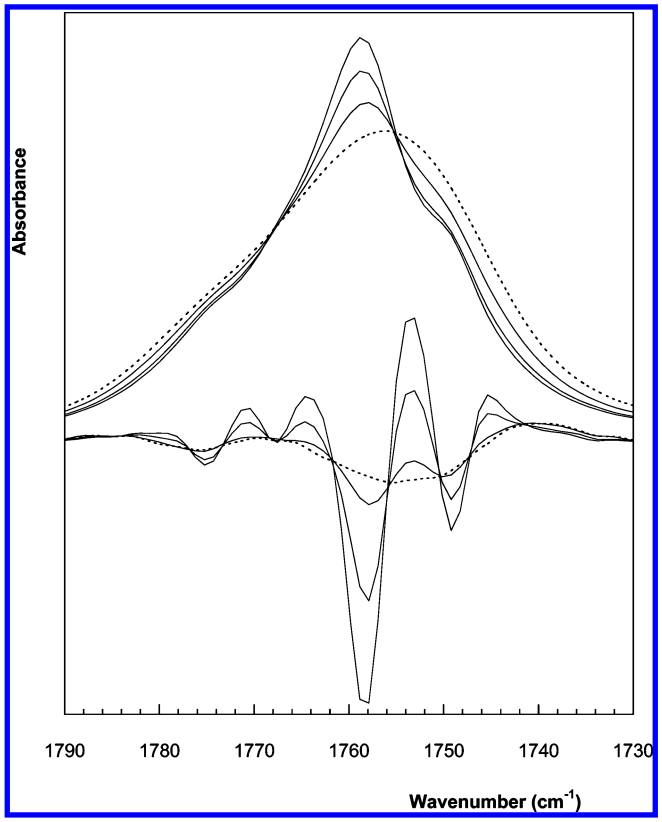

Figure 5. Carbonyl stretching region of PLLA (upper side spectra) and second derivatives (bottom side spectra) recorded during isothermal crystallization at 150 °C. The spectrum of amorphous PLLA is highlighted with a dotted line.

derivative spectrum of PLLA during crystallization splits into four peaks located at 1776, 1767, 1759, and 1749 cm^{-1} (Figure 5).

The crystallization process of polylactides has also been studied by other researchers,[14,46] and at this point we consider it interesting to discuss the results reported by Zhang et al.[14] during the melt crystallization of PLLA. By subtraction procedures they detected up to four components in the difference spectra; the single positive lobe was assigned to the crystalline phase, and the three negative lobes to the amorphous phase. They attributed the complex shape of this spectral region to correlation field splitting arising from interchain dipole−dipole interaction between C═O groups.[14] However, it is well-known that splitting due to the correlation field is only possible for the crystalline phase.[15] Hence, the correlation field splitting interpretation is not consistent with experimental results because the difference in spectra should show multiplicity in positive lobes corresponding to the crystalline phase. The correlation field splitting hypothesis also can be rejected since it is only observed at room temperature in the ($-CH_2-$) bending vibrations and in the ($-CH_2-$) rocking mode; but not in the C═O stretching region.[15] In conclusion, the correlation field splitting hypothesis does not explain the splitting observed in the C═O band, nor the band observed at 1776 cm^{-1} by second derivative techniques.[47] Thus, we will follow our analysis of the C═O stretching region considering only intramolecular coupling and possible intermolecular TDC interactions.

The four peaks located at about 1776, 1767, 1759, and 1749 cm^{-1} are a result of the crystallization process, hence must be attributed to material within the spherulites. Of course, the amorphous material between growing spherulites remains in its initial amorphous state, and should give a spectrum similar to the initial one. Thus, during the crystallization process the C═O spectral region can be interpreted as the overlap of two broad amorphous bands attributed to amorphous material between spherulites, and four narrow bands attributed to material within the spherulites. Because derivative techniques enhance the intensity of narrow bands, these four peaks can be easily discerned in the second derivative spectra even from the initial stages of crystallization. However, at the end of the crystallization process, the whole space is filled with spherulites, and the spectrum should be comprised of the four bands attributed to them. The intensity of the peak at 1759 cm^{-1} increases noticeably during crystallization, and is thus assigned to the crystalline phase, built from gt conformers.[7] In addition, as gt conformers in the interlamellar region should absorb at a similar wavenumber, it certainly should be attributed to the overlapped absorption of gt conformers in the amorphous and crystalline phases. As before, the band at 1776 cm^{-1} is attributed to the gg conformers in the interlamellar region. According to the SCO model (Figure 4), the new bands at 1749 and 1767 cm^{-1} can be attributed to tt and tg conformers, respectively. These assignments are listed in Table 1.

TABLE 1: Assignments for the Spectral Bands Observed in the C═O Stretching Region[a]

location (cm^{-1})	assignment
1776.2	gg interphase
1767.3	tg interphase
1759.0	gt crystalline + gt interphase
1749.1	tt interphase

[a] Peak locations have been obtained from curve fitting analysis of crystalline PLLA at 30 °C (see Figure 6).

In this initial assignment, spectral shifts related to intermolecular TDC interactions have not been considered, because they can be discarded for the following reasons. The influence of TDC interactions on frequency shifts of ordered phases has been studied in PTFE, POM, and POE by Kobayashi et al.[25,26] They proved that IR bands perpendicular to the helical axis of these polymers do not show morphology dependent frequency shifts related to TDC interactions, because the transition moments are canceled out when they are summed up over the whole crystallite.[25,26] As the crystalline band at 1759 cm^{-1} corresponds to a perpendicular mode, it should not be shifted by TDC interactions. Regarding the amorphous contributions, it is accepted that in disordered phases TDC interactions do not cause any spectral shift because transition dipoles surrounding any location are randomly arranged. However, this is only a first-order approximation, because certain spatial orientation can be expected through dipole−dipole interactions. Fortunately, tg, gt, and tt conformers show again their transition moments in the perpendicular direction to the helical chain, and for similar reasons to those reported above, their absorption bands should not be shifted by TDC interactions. A higher sensibility to TDC interactions can be expected for the band at 1776 cm^{-1}. In fact, the location of this band varies from 1775 to 1777 cm^{-1} depending on temperature and crystallinity, while the remaining bands shift below 0.3 cm^{-1} in the same experimental conditions. Hence, we conclude that intermolecular TDC interactions shift only slightly the band attributed to gg conformers.

A tentative spectral curve fitting of the C═O spectral region of crystalline PLLA (Figure 6) suggests that this spectral region can be adequately fit to individual bands with a half-height width of about 8.6 cm^{-1}. A similar width for all the individual components is also suggested by the similar widths observed for the second derivative peaks. Obtained peak locations and assignments are listed in Table 1. However, note that quantitative information seems difficult to extract because the band at 1759

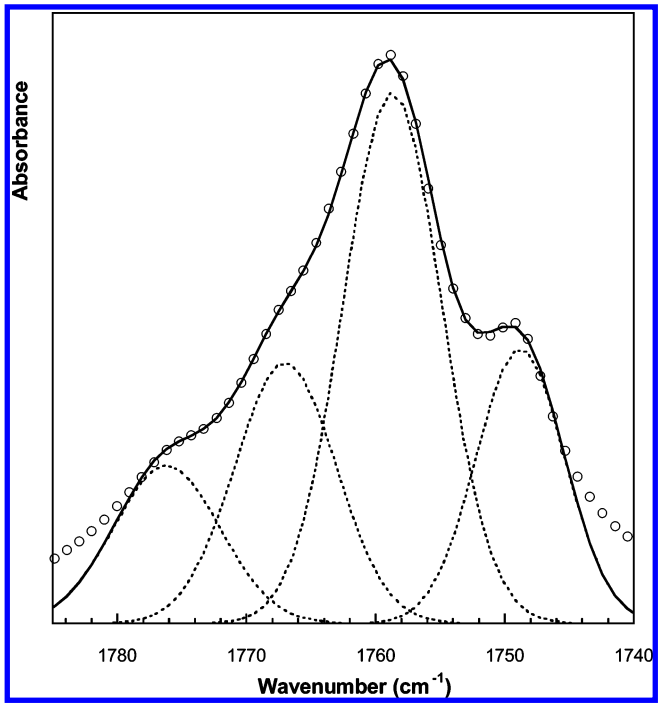

Figure 6. Carbonyl stretching region of PLLA at room temperature after isothermal crystallization for an hour at 150 °C, followed by slow cooling to room temperature. Experimental spectrum (open points), curve fitting components (dotted lines), and total sum (continuous line).

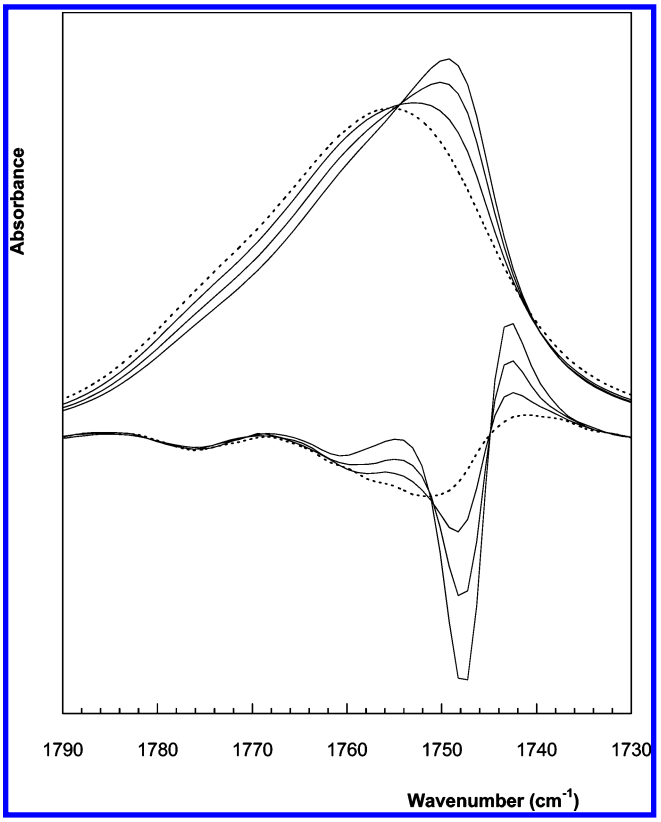

Figure 7. Carbonyl stretching region of PLLA/PDLA stereocomplex (upper side spectra) and second derivatives (bottom side spectra) recorded during isothermal crystallization at 190 °C. The spectrum of the completely amorphous blend is highlighted with a dotted line.

cm^{-1} is in fact the sum of two overlapped contributions, attributed to gt conformers in the lamellae and in the interlamellar phases.

The occurrence of such narrow bands can be explained by recalling recent findings in crystallization studies. Traditional crystallization theories assume a switchboard crystallization pattern for polymers crystallized from the melt, in which three phases are discerned: the crystalline phase, the interphase, and the amorphous phase.[48−50] The interphase material is considered a metastable material with a typical thickness of about 1−2 nm, but most studies are based on flexible polymers (typically poly(ethylene) chains). Recent investigations on polymers with stiff chains support interlamellar regions devoid of random characteristics.[51,52] According to computational studies based on lattice models, the structure of the interphase strongly depends on the tight-fold energy, E_η, a parameter introduced to account for the energy expenditure required to form a tight fold.[52,53] The interphase thickness increases with the value of E_η, up to the point of persisting over several lattice layers away from the crystal surface. In addition, experimental TEM results on lamellar semicrystalline poly(ethylene terphthalate) show that the crystalline order appears to be dissipated at distances greater than the average thickness of the interlamellar noncrystalline layer.[52] Similarly to PET, the backbone chain of PLLA is stiff,[54] as confirmed by its characteristic ratio, $C_\infty = 11.8$,[55] and a broad interphase can be expected. Hence, the narrow spectral contributions observed in the C═O stretching region can be attributed to semiordered material in the interlamellar region. Note that according to general IR theory the only explanation supporting the occurrence of narrow bands is the existence of ordered or semiordered phases; any interpretation based on specific interactions should point in the opposite direction.[27]

The small influence of intermolecular TDC interactions in the shape of the C═O stretching spectral region gains additional support by observing the spectral changes observed during crystallization of the stereocomplex of PLLA with PDLA (the optical isomer of PLLA) in Figure 7.[12] As can be seen, crystallization promotes a new spectral band at 1748 cm^{-1}, attributed to the crystalline stereocomplex. It was proved[12] that this spectral contribution is shifted to lower wavenumbers due to C−H···O═C hydrogen bonding. The key point is that band splitting is not observed during crystallization, and the bands attributed to the initial amorphous phase maintain their original shape during the ordering process. Note that both PLLA and its stereocomplex crystallize in helical conformations of similar geometry, and this result cannot be attributed to different helical geometries. If TDC interactions were responsible for the splitting observed during crystallization of PLLA, they should also be observed in the stereocomplex. In fact, enhanced interactions should be expected in the stereocomplex because TDC interactions are transmitted through hydrogen bonds, as confirmed in studies of polyglycine.[16,17] The absence of spectral shifts related to TDC interactions during crystallization of the stereocomplex seems clear. According to our interpretation, the shape of this spectral region can be explained by simply assuming different crystallization mechanisms for PLLA and its stereocomplex, so that the interlamellar material in the PLLA/PDLA stereocomplex remains in a truly random phase during crystallization.

Another important point in this study is the dispersion curve for the C═O stretching region of PLLA. According to developed theory,[41] for a system of coupled oscillators the relation between absorption frequency and phase angle is

$$\nu_k^2 = \nu_0^2 + 2\sum_i H_i \cos(i\phi_k) \qquad (10)$$

where ν_k is the absorption frequency for the kth normal mode, ν_0 is the absorption frequency for the uncoupled oscillator ($\phi = 90°$), H_i is an interaction parameter, and the summation

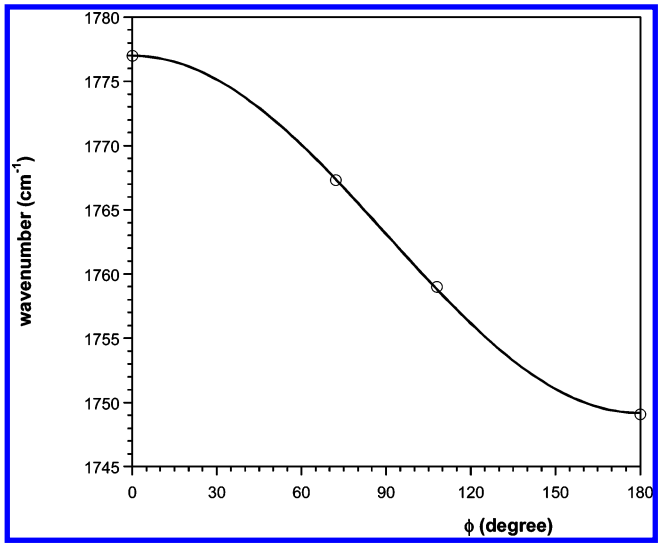

Figure 8. Dispersion curve for the C═O stretching region of PLLA, interpolated according to eqs 10 and 11. Both equations match the same curve.

extends to the number of different groups involved in the coupling interaction. In the simplest case, it can be assumed that coupling between C═O groups is the main contribution to the dispersion curve, the influence of backbone vibrations being a second-order effect, hence $i = 1$. In this case, the coupling parameter can be approximated to $H_1 = \nu_0\Delta\nu$, where $\Delta\nu$ is the frequency difference between the in-phase mode and the unperturbed mode. Figure 8 displays the fit of experimental data to eq 10, and the dispersion curve interpolated assuming the validity of eq 10. Peak locations have been taken from Table 1, except in case of gg conformers, for which a value of 1777 cm^{-1} obtained from the amorphous spectrum at room temperature is adopted because of the lower influence of TDC interactions. Corresponding phase angles are 0° (gg), 72° (tg), 108° (gt), and 180° (tt). The fit of experimental data to eq 10 is excellent ($R = 0.99994$), and the values obtained for ν_0 and H_1 are 1763.1 cm^{-1} and 24 500 cm^{-2}, respectively ($\Delta\nu = 13.9$ cm^{-1}).

The validity of eq 10 in PLLA could be questioned because, as discussed earlier, mechanical coupling should account only for a certain portion of the carbonyl−carbonyl interaction. Miyazawa developed a first-order perturbation theory that can be considered a more general treatment.[56,57] He obtained a simple equation relating phase angles and absorption wavenumbers:

$$\nu(\delta,\delta') = \nu_0 + \sum_s D_s \cos(s\delta) + \sum_{s'} D_{s'} \cos(s'\delta') \quad (11)$$

where ν_0 is the unperturbed frequency, the second and third terms are due to the intrachain and interchain vibrational interactions, respectively, δ is the phase angle between adjacent group motions in the chain, and D_s is determined by the potential and kinetic energy interactions between the sth neighbors in the chain. This equation has been widely applied in polypeptides assuming neighboring intrachain perturbations and interchain perturbations through hydrogen bonds.[16,17] Similarly, it can be applied to PLLA neglecting the interchain term to be consequent with the intramolecular origin assumed for the coupling interaction. Fitting of this equation to the same data as above gives a curve that matches the previous one ($R = 0.99993$). Both curves are displayed in Figure 8 but cannot be discerned (if the square of Miyazawa's equation is calculated, it renders eq 10 plus an additional negligible term). Obtained fitting parameters are $\nu_0 = 1763.1$ cm^{-1} and $D_1 = 13.9$ cm^{-1}. As expected, both models predict similar trends when intramolecular interactions (through-bonds and through-space intramolecular TDC interactions) are studied.

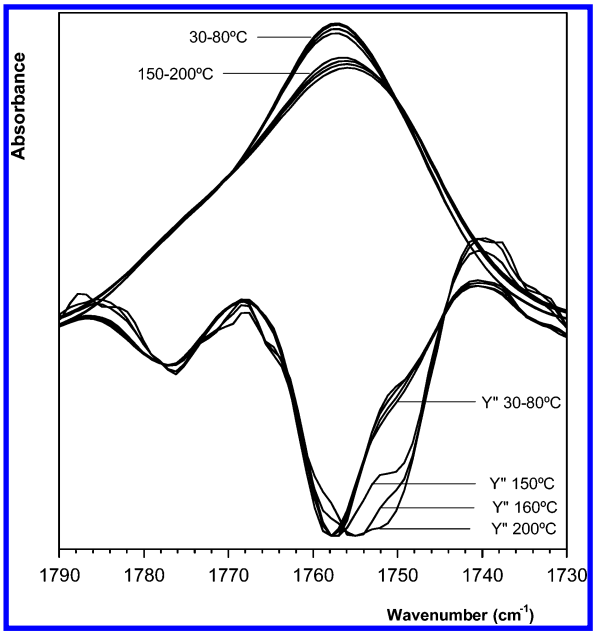

Figure 9. Upper side: Changes with temperature in the C═O stretching region of amorphous PLLA. Bottom side: Autoscaled second derivative spectra. The spectra between 30 and 60 °C are completely identical, changes begin above 60 °C.

C. C═O Stretching Region of Amorphous PLLA. The C═O stretching region of amorphous PLLA also displays unusual changes with temperature (Figure 9) that seem easier to understand after the discussion of the crystalline spectral region. As can be seen in Figure 9, the C═O band remains unaltered from 30 to 60 °C, but at higher temperatures its intensity at about 1759 cm^{-1} decreases, and simultaneously the band widens to lower wavenumbers. In addition, the total area shows a negligible change, below 1%. Second derivative spectra increase the resolution of any spectral band and allow a correct interpretation of these spectral changes. At room temperature, the second derivative spectrum shows two peaks at 1777 and 1758 cm^{-1}, accompanied by an additional contribution at lower wavenumbers (Figure 9). This shoulder is located at about 1749 cm^{-1}, and its contribution increases notably at higher temperatures; in fact, at temperatures above 170 °C it is the dominant contribution in the second derivative spectra. The shoulder observed in the second derivative spectrum at room temperature can be assigned to tt conformers, and the relative intensity of the band suggests a composition exceeding 4% value calculated by Tonelli et al.[8] The spectral changes observed on heating can be attributed to a change in the population distribution of conformers as temperature increases, according to[8]

$$w/w_{gt} = A \exp[-(E - E_{gt})/RT] \quad (12)$$

where w/w_{gt} represents the relative probability of a certain conformer relative to the lowest energy gt conformers, and ($E - E_{gt}$) is the conformational energy difference.

For a quantitative calculation of relative populations of conformers, a curve fitting analysis can be performed. Because bands are highly overlapped, some assumptions are necessary. Second derivative spectra of crystalline PLLA show nearly invariant peak locations with temperature (spectral shifts in the

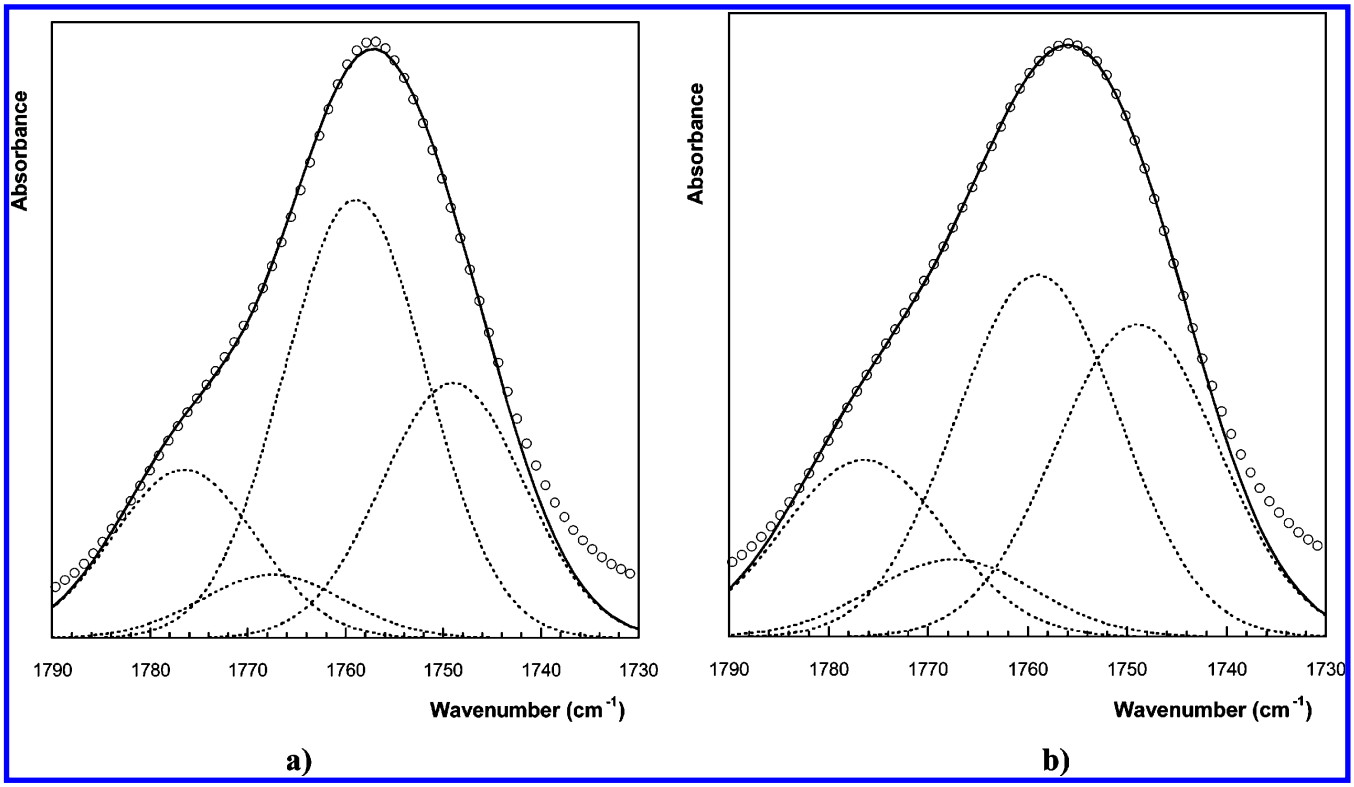

Figure 10. Curve fitting results for amorphous PLLA at (a) 30 and (b) 180 °C. Peaks have been fitted assuming the same half-height width for the four components, and peak locations have been fixed to 1776.5, 1767.5, 1759, and 1749 cm^{-1}.

TABLE 2: Curve Fitting Results for Amorphous PLLA in the Temperature Range from 30 to 200 °C[a]

temp (°C)	width (cm^{-1})	% area			
		gg conf	tg conf	gt conf	tt conf
30	17.1	18.2	6.8	47.4	27.6
40	17.1	18.1	7.0	47.2	27.7
50	17.1	18.1	7.0	47.2	27.7
60	17.1	18.1	7.1	47.1	27.8
70	17.2	18.1	7.3	46.6	28.0
80	17.5	18.3	7.3	46.6	27.8
150	19.0	19.0	7.7	41.4	32.0
160	19.2	19.0	8.1	40.0	32.9
170	19.2	19.0	8.2	39.4	33.3
180	19.3	19.0	8.3	39.0	33.7
190	19.2	18.9	8.8	38.3	33.9
200	19.4	19.1	8.4	38.6	33.9

[a] Peak locations have been fixed at 1776.5, 1767.5, 1759, and 1749 cm^{-1}. The resulting common band width is also shown.

temperature range 80−150 °C are below 0.3 cm^{-1}, except for gg conformers). Band positions have been fixed to the mean locations obtained by curve fitting of amorphous and crystalline PLLA in the temperature range 30−150 °C: 1776.5, 1767.5, 1759, and 1749 cm^{-1}. Also, the same width has been assumed for all bands. Thus, for reliability reasons, the problem has been simplified to the fitting of four intensities and a single width. Good fits have been obtained for all temperatures, and Figure 10 shows the fitting match at 30 and 180 °C. The conformer population distribution at different temperatures is shown in Table 2. As can be seen, the population of gg conformers at room temperature is lower than that suggested by Tonelli et al.,[8] in agreement with recent studies.[9] However, the population of tt conformers is higher than theoretically predicted, as expected according to the shape of the second derivative spectrum. In the case of tg conformers, small relative populations are obtained, as suggested by Tonelli.[8] At higher temperatures, the population of tt conformers increases, and this is the main reason for the observed spectral band broadening and shifting to lower wavenumbers.

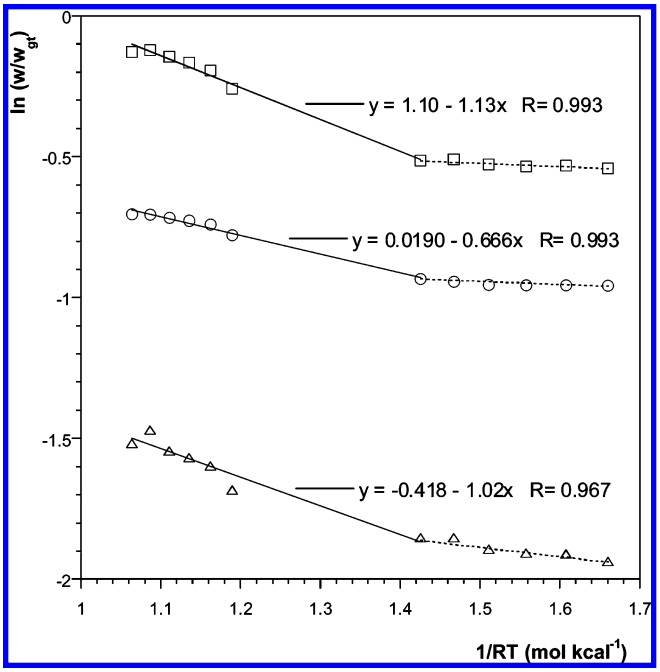

Figure 11. Arrhenius plots for the conformer population distribution: (□) tt conformers, (○) gg conformers, and (△) tg conformers. The continuous line is the linear regression from 80 to 200 °C, and the discontinuous line is a guide to visualize the change of slope.

Curve fitting analysis results can be used to calculate energy differences and preexponential factors according to eq 11. The Arrhenius type plot is shown in Figure 11, and obtained parameters are presented in Table 3, together with theoretical values reported by Tonelli et al.[8] Calculated values for tg conformers must be taken with caution because of the high error

TABLE 3: Energy Differences and Preexponential Factors Obtained at Temperatures between 80 and 200 °C[a]

location (cm^{-1})	conformer	ΔE (kcal/mol)	A
1776.5	gg	0.67 (0.08)	1.0 (0.77)
1767.5	tg	1.02 (1.40)	0.68 (0.77)
1759	gt		
1749	tt	1.13 (1.52)	3.0 (1.0)

[a] Theoretical values obtained by Tonelli et al. are shown in parentheses for reference.

that can be expected due to the low relative intensity of this spectral contribution. However, values obtained for gg and tt conformers seem quite reliable because the fitting procedure shows only a limited influence on them. Comparing these values to Tonelli's calculations, an important energetic deviation is observed for gg conformers (0.67 kcal/mol experimental, versus 0.08 kcal/mol theoretical). A similar value was proposed by Yang et al.[9] from studies of experimental and simulated Raman spectra. In addition, the theoretical energy differences[8] for tg and tt conformers are about 0.4 kcal/mol higher than experimental values. Nevertheless, the high discrepancies obtained for the population of tt conformers are mainly due to the difference in the preexponential factor obtained from both methods, as the experimental value is three times higher than the theoretical one. From a theoretical point of view, the preexponential factor reflects the relative breadths of the minima in conformational energy maps, or relative population degeneracies.[8] Thus, FTIR results indicate that the relative width of the tt minimum in the conformational energy map is considerably higher than that reported in Tonelli's paper.[8]

Conclusions

The carbonyl stretching region of PLLA shows conformational sensitivity and the number and location of the observed bands can be correctly interpreted assuming intramolecular coupling as the main reason for the observed splitting and spectral shifts. Intermolecular transition dipole coupling (TDC) interactions seem to play only a minor role: only the absorption bands in the direction of the helical chain, attributed to gg conformers, shift slightly. To aid in the interpretation of the observed spectral features, the SCO model was adopted. This model predicts adequately the observed intensity ratios for the symmetric and asymmetric bands of dicarbonyl compounds. It also reproduces the dispersion curves predicted by more general treatments such as Miyazawa's first-order perturbation theory. Hence, the SCO model is adopted here as an adequate yet simple tool for the interpretation of band splitting caused by intramolecular coupling of polylactide.

During crystallization of PLLA, new bands develop in the C═O spectral region. At these initial stages, the bulk sample consists of growing spherulites separated by an amorphous phase, and the infrared spectrum can be considered as the sum of the spectra corresponding to both regions. At the end of the crystallization process, spherulites fill the whole space, and the spectrum shows narrow bands that can be attributed to gg, tg, gt, and tt conformers. The SCO model predicts a single band for each conformer, because C═O groups orient only parallel to the helix axis (gg conformers) or perpendicular to it (gt, tg, and tt conformers). Hence, the A mode is not observed for the crystalline polymer in the 10_3 helical conformation. The C═O stretching band of the crystalline polymer shows very narrow contributions, with a half-height width of about 9 cm^{-1}. Such narrow band results can be attributed only to highly ordered material, suggesting that the interlamellar material adopts a highly ordered state. In agreement with recent theoretical models, our results are consistent with the existence of a metastable semiordered interphase material, a feature proved in few systems with stiff chains.

The carbonyl spectral region of the amorphous polymer has been studied at different temperatures and information regarding the conformer population distribution at different temperatures has also been obtained. In agreement with recent studies the population of gg conformers is lower than that theoretically predicted. In addition, our study also indicates a higher population of tt conformers, mainly due to a higher preexponential factor than the one reported by Tonelli et al. These conformers give extended chains, and should not be in contradiction with the stiffness shown by PLLA chains.

Acknowledgment. The authors are thankful for financial support from the Basque Government (Department of Industry, Trade and Tourism (project IE03-105)) and from MCYT (Project MAT2005-08347-C02-01). They would also like to acknowledge the collaboration of other members of CIC biomaGUNE and the support from the BIOBASK Agency.

References and Notes

(1) Doi, Y. *Microbial Polyesters*; VCH Publishers: New York, 1990.
(2) Lunt, J. *Polym. Degrad. Stab.* **1998**, 59, 145−152.
(3) Zhu, K. L.; Xiangzhou, L.; Shilin, Y. *J. Appl. Polym. Sci.* **1990**, *39*, 1.
(4) Bergsma, J. E.; Bos, R. R. M.; Rozema, F. R.; Jong, W. D.; Boering, G. *J. Mater. Sci.*: *Mater. Med.* **1996**, *7*, 1.
(5) Fambri, L.; Pergoretti, A.; Fenner, R.; Incardona, S. D.; Migliarisi, C. *Polymer* **1997**, *38*, 79.
(6) Sinclair, R. G. *Pure Appl. Chem.* **1996**, *A33*, 585.
(7) Hoogsteen, W.; Postema, A. R.; Pennings, A. J.; Brinke, G. T.; Zugenmaier, P. *Macromolecules* **1990**, *23*, 634.
(8) Brant, D. A.; Tonelli, A. E.; Flory, P. J. *Macromolecules* **1969**, *2*, 228.
(9) Yang, X.; Kang, S.; Hsu, S. L.; Stidham, H. D.; Smith, P. B.; Leugers, A. *Macromolecules* **2001**, *34*, 5037.
(10) Kister, G.; Cassanas, G.; Vert, M. *Polymer* **1998**, *39*, 267.
(11) Meaurio, E.; Zuza, E.; Sarasua, J. R. *Macromolecules* **2005**, *38*, 1207.
(12) Sarasua, J. R.; López, N.; López, A.; Meaurio, E. *Macromolecules* **2005**, *38*, 8362.
(13) Zhang, J.; Sato, H.; Tsuji, H.; Noda, I.; Ozaki, Y. *J. Mol. Struct.* **2005**, *735*, 249.
(14) Zhang, J.; Tsuji, H.; Noda, I.; Ozaki, Y. *J. Phys Chem. B* **2004**, *108*, 11514.
(15) Lagaron, J. M. *Macromol. Symp.* **2002**, *184*, 19.
(16) Moore, W. H.; Krimm, S. *Proc. Natl. Acad. Sci. U.S.A.* **1975**, *72*, 4933.
(17) Krimm, S.; Bandekar, J. *Adv. Protein Chem.* **1986**, *38*, 181.
(18) Hamm, P.; Woutersen, S. *Bull. Chem. Soc. Jpn.* **2002**, *75*, 985.
(19) Brauner, J. W.; Flach, C. R.; Mendelsohn, R. *J. Am. Chem. Soc.* **2005**, *127*, 100.
(20) Snyder, R. G.; Maroncelli, M.; Strauss, H. L.; Hallmark, V. M. *J. Phys. Chem.* **1986**, *90*, 5623.
(21) Coleman, M. M.; Graf, J. F.; Painter, P. C. *Specific Interactions and the Miscibility of Polymer Blends*; Technomic Publishing Inc.; Lancaster, PA, 1991.
(22) Iogansen, A. V. *Spectrochim. Acta, A* **1999**, *55*, 1585.
(23) Rozenberg, M.; Loewenschuss, A.; Marcus, Y. *Phys. Chem. Chem. Phys.* **2000**, *2*, 2699.
(24) Taylor, R.; Kennard, O. *J. Am. Chem. Soc.* **1982**, *104*, 5063.
(25) Kobayashi, M.; Sakashita, M. *J. Chem. Phys.* **1992**, *96*, 748.
(26) Kobayashi, M.; Sakashita, M.; Adachi, T.; Kobayashi, M. *Macromolecules* **1995**, *28*, 316.
(27) Painter, P. C.; Coleman, M.; Koening, J. L. *The theory of vibrational spectroscopy and its application to polymeric materials*; Wiley: New York, 1982; p 383.
(28) Popov, E. M.; Khomenko, A. K.; Shorygin, P. P. *Ser. Khim.* **1965**, *1*, 51.
(29) Fayat, C.; Foucaud, A. *Bull. Soc. Chim. Fr.* **1971**, *3*, 987.
(30) Vledder, H. J.; Van Kleef, F. S. M.; Mijlhoff, F. C.; Leyte, J. C. *J. Mol. Struct.* **1971**, *10*, 189.
(31) Davison, W. H. T. *J. Chem. Soc., Abstr.* **1951**, 2456.

(32) Kleinpeter, E.; Klod, S.; Perjéssy, A.; Šamaliková, M.; Synderlata, K.; Šusteková, Z. *J. Mol. Struct.* **2003**, *645*, 17−27.
(33) Schindler, A.; Harper, D. H. *J. Polym. Sci., Polym. Chem. Ed.* **1979**, *17*, 2593.
(34) Savitzky, A.; Golay, M. J. E. *Anal. Chem.* **1964**, *36*, 1627−1639.
(35) Steiner, J.; Termonia, Y.; Deltour, J. *Anal. Chem.* **1972**, *44*, 1906−1909.
(36) Kang, S.; Hsu, S. L.; Stidham, H. D.; Smith, P. B.; Leugers, M. A.; Yang, X. *Macromolecules* **2001**, *34*, 4542.
(37) *ArgusLab 4.0*; Thompson, M. A. (mark@arguslab.com); Planaria Software LLC: Seattle, WA (http://www.arguslab.com).
(38) Theimer, O. *J. Chem. Phys.* **1957**, *27*, 408.
(39) Zbinden, R. *J. Mol. Spectrosc.* **1959**, *3*, 654.
(40) Snyder, R. G. *J. Mol. Spectrosc.* **1960**, *4*, 411.
(41) Snyder, R. G.; Schachtschneider, J. H. *Spectrochim. Acta* **1963**, *19*, 85.
(42) Vansanthan, N.; Murthy, N. S.; Bray, R. G. *Macromolecules* **1998**, *31* 8433.
(43) Yoshioka, Y.; Tashiro, K.; Ramesh, C. *J Polym. Sci., Polym. Phys.* **2003**, *41*, 1294.
(44) Cho, H. G.; Strauss, H. L.; Snyder, R. G. *J. Phys. Chem.* **1992**, *96*, 5290.
(45) Hsu, S. L.; Reynolds, N.; Bohan, S. P.; Strauss, H. L.; Snyder, R. G. *Macromolecules* **1990**, *23*, 4565.
(46) Zhang, J.; Tsuji, H.; Noda, I.; Ozaki, Y. *Macromolecules* **2004**, *37*, 6433.
(47) Zhang, J.; Sato, H.; Tsuji, H.; Noda, I.; Ozaki, Y. *Macromolecules* **2005**, *38*, 1822.
(48) Flory, P. J. *Principles of Polymer Chemistry*; Cornell University Press: Ithaca, NY, 1953.
(49) Mandelkern, L. *An Introduction to Macromolecules*; Springer-Verlag: New York, 1983.
(50) Mandelkern, L. *Crystallization in Polymers*; McGraw-Hill Book Co.: New York, 1983.
(51) Ivanov, D. A.; Pop, T.; Yoon, D. Y.; Jonas, A. M. *Macromolecules* **2002**, 35, 9813.
(52) Rastogi, A.; Terry, A. E.; Mathot, V. B. F.; Rastogi, S. *Macromolecules* **2005**, *38*, 4744.
(53) Flory, P. J.; Yoon, D. Y.; Dill, K. A. *Macromolecules* **1984**, 17, 862.
(54) Urayama, H.; Moon, S. I.; Kimura Y. *Macromol. Mater. Eng.* **2003**, *288*, 137.
(55) Joziasse, C. A.; Veenstra, H.; Grijpma, D. W.; Pennings, A. *J. Macromol. Chem. Phys.* **1996**, *197*, 2219.
(56) Miyazawa, T. *J. Phys. Chem.* **1960**, *32*, 1647.
(57) Miyazawa, T.; Blout, E. R. *J. Am. Chem. Soc.* **1961**, *83*, 712.